Evolving Motility of Active Droplets Is Captured by a Self-Repelling Random Walk Model

Wenjun Chen,[1] Adrien Izzet,[1,2] Ruben Zakine,[1,3,4] Eric Clément,[5,6] Eric Vanden-Eijnden,[3] and Jasna Brujic[1,5,*]
[1]Center for Soft Matter Research, Physics Department, New York University, New York, New York 10003, USA
[2]Université Paris-Saclay, INRAE, AgroParisTech, UMR SayFood, 91120 Palaiseau, France
[3]Courant Institute, New York University, 251 Mercer Street, New York, New York 10012, USA
[4]LadHyX UMR CNRS 7646, École Polytechnique, 91128 Palaiseau Cedex, France
[5]Laboratoire PMMH-ESPCI Paris, PSL University, Sorbonne University, 7, Quai Saint-Bernard, 75005 Paris, France
[6]Institut Universitaire de France (IUF), 75005 Paris, France

(Received 13 May 2024; revised 2 October 2024; accepted 9 December 2024; published 3 January 2025)

In living matter, concentration gradients of nutrients carve the motility of microorganisms in a heterogeneous environment. Here, we use swimming droplets as a model system to study how swimmer-trail interactions guide locomotion. Combining experiments and theory, we show that our non-Markovian droplet model quantitatively captures droplet motility. The two fit parameters provide the first estimate of the effective temperature arising from hydrodynamic flows and the coupling strength of the propulsion force. This framework is general and explains memory effects, droplet hovering, and enhanced collective motion.

DOI: 10.1103/PhysRevLett.134.018301

A common mechanism for chemotaxis of microorganisms is to release, sense, and respond to concentration gradients of nutrients [1–3]. This chemically evolving landscape can be mimicked by swimming droplets to quantitatively study the key ingredients underlying the physical principles of motility in biology. Active droplets are a class of artificial microswimmers that consume energy from the environment to fuel their motility [4–7]. Changing temperature [8,9], viscosity [10,11], droplet size [12–14], fuel concentration [15], or geometric confinement [16] have been shown to lead to different types of droplet motility. Typically, a swimming droplet dissolves into micelles and leaves an oil trail behind, which then creates a repulsive concentration gradient that results in self-avoidance [15,17–20]. As a result, the mean square displacement of these droplets cannot be described by Flory's self-avoiding polymer theory [21] but rather falls into a class of self-interacting random walks [22–24].

Theoretical models that couple chemotactic motion with the diffusing chemical field secreted by the swimmers have been developed [25–31]. They display features such as self-trapping due to chemoattractant clouds [25], enhanced diffusion [26,27], and behavior akin to active Brownian particles [28,31], emphasizing the nuanced interplay of chemical fields and swimmer motion.

Here, we combine experiments and theory to characterize the motion of a single droplet lifetime. Our coarse-grained model captures droplet shrinkage through the use of a mollified delta function [31,32]. Moreover, we take into account the full trail of the droplet to model self-avoidance rather than only local chemical gradients [18,19,33]. Our model quantitatively estimates the self-propulsion force, the level of noise in the system through an effective temperature T_{eff}, as well as the coupling strength β between the droplet and its chemical gradient. The model successfully captures droplet mean square displacements (MSDs) as a function of fuel concentration and explains their hovering in 3D due to a surface interaction. In addition, it predicts many-body effects, such as enhanced diffusion. This model is, therefore, general and directly applies to a wide variety of active systems, including all Marangoni-driven swimmers.

Our experimental system consists of a single droplet of diethyl phthalate (DEP, Sigma) with an initial radius of around 80 μm, which is injected into an aqueous solution of sodium dodecyl sulphate (SDS) [15]. As shown in Fig. 1(a), a droplet immersed in an SDS solution above the critical micelle concentration (CMC) starts dissolving and forms oily micelles homogeneously around the droplet. This symmetry can be spontaneously broken due to fluctuations in the system. Given the fact that there is a difference in the surfactant CMC in DEP-saturated water and pure water, the asymmetry creates a surface tension gradient, giving rise to a Marangoni flow that drives self-sustained droplet motion. The droplet, therefore, leaves a trail of oily micelles as it moves. A snapshot at the end of the trajectory ($t = 90$ s) reveals the evolution of the diffusive trail over time, as shown in Fig. 1(b).

In Fig. 1(c), we show the fluorescence intensity profile at the starting point $\mathbf{X}_0$ of the trajectory. To model trail diffusion, we approximate the droplet as a 3D Gaussian sphere emitting oil, $G_R(\mathbf{x}) = [1/(2\pi R^2)^{3/2}] \exp[-(|\mathbf{x}|^2/2R^2)]$, yielding the

*Contact author: jb2929@nyu.edu

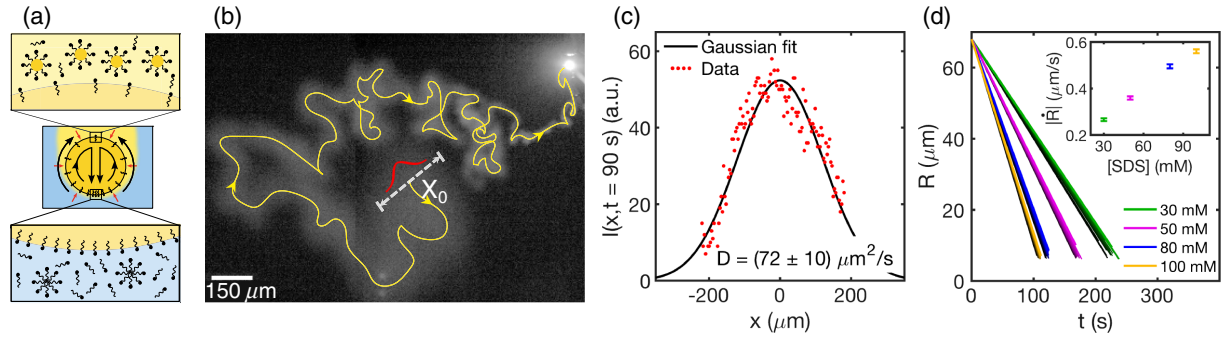

FIG. 1. (a) Schematic of the droplet propulsion mechanism via interfacial Marangoni gradients, including the monopolar flow (red arrows) described in [34]. (b) A snapshot at the end of a swimming trajectory shows the diffusive trail of oily micelles fluorescently labeled with Nile red ($R_0 = 35$ μm, [SDS] = 30 mM). (c) A Gaussian fit using Eq. (1) of the fluorescence intensity [red in (b)] yields the micellar diffusion constant $D = (72 \pm 10)$ μm^2/s. (d) The droplet radius decreases linearly with time, giving a solubilization rate that increases as a function of SDS concentration in the inset.

density profile at position $\mathbf{x}$ around the emission site $\mathbf{X}_0$:

$$c_t(\mathbf{x}) = \frac{c_0}{[2\pi(R^2+2Dt)]^{3/2}} \exp\left(-\frac{|\mathbf{x}-\mathbf{X}_0|^2}{2(R^2+2Dt)}\right), \quad (1)$$

where the initial standard deviation equals the droplet radius R, D is the diffusion constant of the filled micelles, and t is the diffusion time. The intensity in Fig. 1(c) is directly proportional to the concentration field. Fitting the data to Eq. (1) yields $D = (72 \pm 10)$ μm^2/s, which corresponds to the radius of filled micelles (3.4 ± 0.5) nm, consistent with values reported in the literature [35,36]. Measuring droplet radius over time [Fig. 1(d)] shows a linear decrease: $R_t = R_0 - |\dot{R}|t$, where $|\dot{R}| = cst$ is the shrinkage rate of the droplet radius. The shrinkage rate is related to the droplet oil emission rate $\alpha_t \simeq (3R_t^2/\delta^3)|\dot{R}|$, where δ is the size of the oil sphere in the micelle, approximated by the micellar radius. With increasing SDS concentration, the shrinkage rate increases, as shown in the inset.

At [SDS] = 80 mM, Figs. 2(a) and 2(b) show single droplet trajectories over their lifetime. To quantify the time evolution of the trajectories, we compare the ensemble-averaged MSD for different sections of the trajectory [Fig. 2(b)]:

$$\mathrm{MSD}_t^{\mathrm{ens}} = \frac{1}{N}\sum_{i=1}^{N}\left|\mathbf{X}_{t+t_0}^{(i)} - \mathbf{X}_{t_0}^{(i)}\right|^2, \quad (2)$$

where t_0 is the starting time and N is the number of trajectories indexed by i. The top panel shows the change in the MSD as a function of the initial radius at which the section begins. As a result of this non-Markovian behavior, the bottom panel shows a discrepancy between the ensemble-averaged and the time-averaged MSD:

$$\mathrm{MSD}_t^{\mathrm{time}} = \frac{1}{N(M_t+1)}\sum_{i=1}^{N}\sum_{j=0}^{M_t}\left|\mathbf{X}_{t+j\Delta t}^{(i)} - \mathbf{X}_{j\Delta t}^{(i)}\right|^2, \quad (3)$$

where τ is the time length of each trajectory, $\Delta t = 0.02$ s, and $M_t = \lfloor(\tau - t)/\Delta t\rfloor$.

To explain these phenomena, we employ a non-Markovian droplet model in which complex hydrodynamics and chemo-advection mechanisms are represented as a fundamental coupling between chemical gradients and droplet motion. In this model, the time-evolving oil field $c_t(\mathbf{x})$ is governed by a 3D diffusion equation, while the droplet motion is described by a stochastic differential equation with a constant noise amplitude σ corresponding to the hydrodynamic fluctuations generated by the dissolving droplet:

$$\partial_t c_t(\mathbf{x}) = D\nabla^2 c_t(\mathbf{x}) + \alpha_t G_{R_t}(\mathbf{x} - \mathbf{X}_t), \quad (4a)$$

$$\gamma_t \dot{\mathbf{X}}_t = -\beta\frac{R_t^3}{\delta^3}\int_{\mathbb{R}^3} G_{R_t}(\mathbf{x} - \mathbf{X}_t)\nabla c_t(\mathbf{x})d\mathbf{x} + \sqrt{\sigma}\xi_t. \quad (4b)$$

The integral is performed in 3D, using the reflecting boundary condition modeled by an image droplet on the bottom of the sample cell (see Supplemental Material [37]). Equation (4a) has a diffusion term employing the experimentally determined D of the oily micelles and a source term that depends on the instantaneous position $\mathbf{X}_t$ of the moving droplet emitting oil at a rate of α_t. Equation (4b) is a modified Langevin equation for a Brownian particle in a force field with the inertial term neglected in the low-Reynolds number regime. The friction coefficient is given by $\gamma_t = 6\pi\eta R_t$, where η is the viscosity of the aqueous phase. The droplet response to the concentration gradient is defined as a convolution of the concentration gradient with the mollified delta function, multiplied by $\beta R_t^3/\delta^3$, with β as the coupling strength and R_t^3/δ^3 denoting the amount of oil carried by the droplet. Note that the force depends on both the gradient of the oil field and R_t^3/δ^3. The droplet emits the oil volumetrically from the interior and the response to the Marangoni forcing occurs inside and

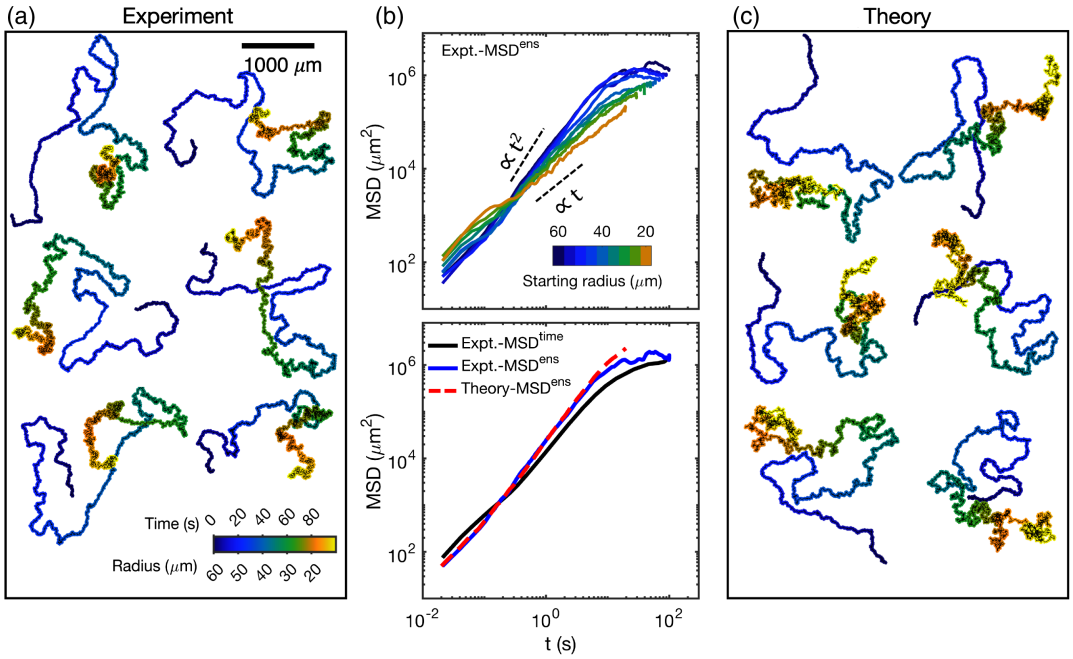

FIG. 2. (a) Experimental trajectories at [SDS] = 80 mM. (b) Top: $\mathrm{MSD}^{\mathrm{ens}}$ of experimental data show dependence on the size range of the shrinking droplet. Bottom: $\mathrm{MSD}^{\mathrm{ens}}$ (blue line) at a starting radius 60 μm shows a discrepancy from the $\mathrm{MSD}^{\mathrm{time}}$ (black line), indicating memory effects. The model fits the data very well (except for the plateau arising from sample-cell confinement) with $\beta = 0.038 k_B T M^{-1}$, where $M \equiv \mathrm{mol/L}$ and $T_{\mathrm{eff}} = 8 \times 10^4 T_{\mathrm{bath}}$. (c) Model-generated trajectories display the same features as experimental ones shown in (a).

outside the droplet [38–40], such that the propulsion force depends on R^3.

To eliminate the oil field, we can integrate Eq. (4a) to obtain

$$c_t(\mathbf{x}) = \int_0^t \frac{\alpha_s \exp\left(-\frac{|\mathbf{x}-\mathbf{X}_s|^2}{2[R_s^2+2D(t-s)]}\right)}{2\pi[R_s^2+2D(t-s)]^{3/2}} ds. \tag{5}$$

Note that Eq. (1) is an approximation of Eq. (5) that is valid if the droplet moves fast and if we look at positions $\mathbf{x}$ close to the initial $\mathbf{X}_0$. Inserting Eq. (5) in Eq. (4b) and performing the Gaussian integral over $\mathbf{x}$, we get a closed non-Markovian equation for the position of the droplet:

$$\dot{\mathbf{X}}_t = \omega^2 \int_0^t r_t^2 r_s^2 \frac{\mathbf{X}_t - \mathbf{X}_s}{(r_t^2/2 + r_s^2/2 + D(t-s)/R_0^2)^{5/2}} \times \exp\left(-\frac{|\mathbf{X}_t - \mathbf{X}_s|^2}{2R_0^2(r_t^2 + r_s^2 + 2D(t-s)/R_0^2)}\right) ds + \frac{\sqrt{\sigma}}{\gamma_0 r_t}\xi_t, \tag{6}$$

where $\gamma_0 = 6\pi\eta R_0$, $\omega^2 = (3/16\pi^{3/2}\gamma_0\delta^6)|\dot{R}|\beta$, and $r_t = 1 - |\dot{R}|t/R_0$. The first term on the right-hand side, representing the drift velocity v, is determined by an integral over all of its past, incorporating memory effects. The known or experimentally determined input parameters are $D = 72\ \mu\mathrm{m}^2/\mathrm{s}$, $\delta = 3.4$ nm, initial size $R_0 = 80$ μm, $\eta = 0.89$ mPa · s, and the shrinkage rate $|\dot{R}| = 0.5\ \mu\mathrm{m/s}$. The coupling strength β and the noise amplitude σ are determined by fitting the model to the data [see Eq. (9) in Supplemental Material [37]).

As shown in Fig. 2(b) (bottom panel), the model fits the ensemble-averaged MSD of the data very well. This fit corresponds to short-time diffusive, then ballistic, and finally superdiffusive motility at long times. This evolution is akin to a true self-avoiding walk [41], in which the droplet has a finite probability to cross its own path. Other studies have observed a short-time ballistic, and long-time superdiffusive scaling of the MSDs [10], consistent with a self-avoiding walk, owing to the significantly lower droplet activity in their system.

More specifically, we show quantitative agreement between theory and experiments in terms of the drift velocity (i.e., propulsion force) and the noise term, as shown in Fig. 3. The experimental drift velocity v is obtained by trajectory smoothing, and the experimental noise amplitude $\sqrt{A_t}$ is calculated over the given frame rate (see Supplemental Material [37]). Note that, even though the Péclet number decreases over time, our model assumes a constant level of noise in the system (for a given SDS concentration) and captures the relative increase in the fluctuation amplitude in smaller droplets. As droplets shrink over time, here we show that the drift velocity v decreases, while the noise term dramatically increases.

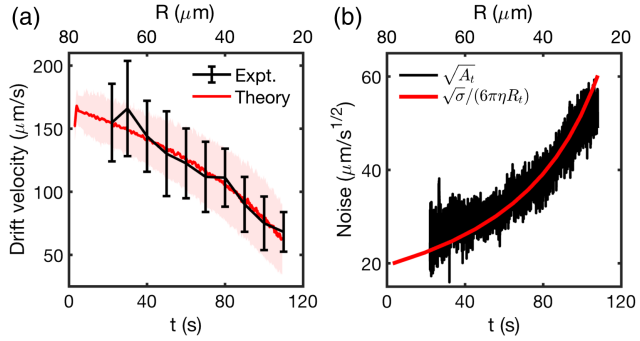

FIG. 3. As the droplet shrinks, the decrease in v in (a) and the increase in $\sqrt{A_t}$ in (b) (see Supplemental Material [37]) are captured by the respective terms on the right-hand side of Eq. (6) using parameters from the MSD fit in Fig. 2(b). Errors in (a) come from averaging over ~100 and 1000 trajectories for experiments and theory, respectively, while the fluctuations in (b) arise from measurement error.

The excellent agreement between the data and the model *a posteriori* justifies the assumed dependence of chemical response on the amount of oil carried by the droplet R_t^3/δ^3 and the assumption of a constant noise amplitude σ.

Next, we vary the SDS concentration to study the effect of shrinkage rate on droplet motility, as shown in Fig. S1 in Supplemental Material [37]. The MSD of our mesoscopic model is in good agreement with experimental data, as shown in Fig. 4(a). As [SDS] increases, the short-time diffusion (noise) in the MSD is suppressed, while the ballistic regime exhibits a decrease in the drift velocity. We speculate that the fast oil solubilization into micelles surrounding the droplets occurs in all directions, leading to reduced Marangoni surface flows, and, therefore, lower speeds, and reduced noise levels (see Fig. S3 in Supplemental Material [37]). Fits to the data give estimates for the noise amplitude σ and the coupling $\tilde{\beta}$ as a function of SDS concentration.

Assuming the noise σ has the same form as white noise $2\gamma_0 k_B T_{\text{eff}}$, with k_B as the Boltzmann constant and T_{eff} as the effective temperature, we find the T_{eff} is 10^5 times the bath temperature [Fig. 4(b)], indicating that thermal fluctuations are not the origin of the noise of the swimmer. As [SDS] increases, both the effective temperature and the instantaneous velocity decrease (see Fig. S4 in Supplemental Material [37]). Hydrodynamic analysis showed that droplets can switch more frequently between dipolar and quadrupolar modes, resulting in more chaotic behavior [10,38,43,44]. However, the exact mechanism for the generation of this noise remains an open question.

The chemical coupling $\tilde{\beta}$ decreases with increasing [SDS] concentration, as shown in Fig. 4(b). Since $\tilde{\beta} = \beta\delta_0^6/\delta^6$, where δ_0 is a constant for dimensionless normalization, this decrease can be attributed to the known increase in the micellar size up to $\sim 1.3\delta$ over our experimental range of [SDS] [42,45,46]. This trend quantitatively explains our results, implying a constant coupling strength $\beta = 0.2 k_B T M^{-1}$.

One manifestation of the coupling strength is that an active droplet is also lifted vertically (in z) against gravity by the self-propulsion force, as shown in Fig. 5(a). As the droplet exudes a spherically symmetric concentration gradient, the presence of the surface boundary breaks this symmetry propelling the droplet upward until the gradient force matches the buoyancy force (~1 nN; see Supplemental Material [37]). Such gradient forces can also enhance droplet settling when aligned with the buoyancy force [47]. The equilibrium height evolves with droplet shrinkage, in agreement with theoretical work [48] and our previous experimental observations [20].

Our model is readily extended to explore collective effects (see Supplemental Material [37]). As shown in Fig. 5(b), ten droplets with an initial size of 80 μm are injected into the center of the sample cell simultaneously. Distinct from the single-droplet scenario, these droplets also are repelled by their neighbors' trails. As a result, the MSD is significantly enhanced, giving rise to a super-ballistic regime [see Fig. 5(c)]. This result highlights the fact that collective phenomena must include the spatio-temporal history of droplet creation.

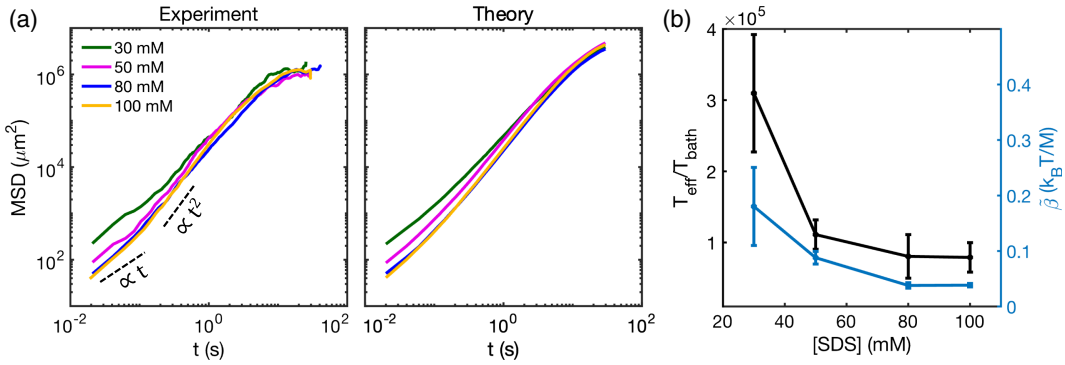

FIG. 4. (a) MSD^{ens} with a starting droplet size of 60 μm shows good agreement between the model and the data as a function of [SDS]. (b) Fitting parameters T_{eff} (black) and coupling $\tilde{\beta} = \beta\delta_0^6/\delta^6$ (blue) decrease as a function of [SDS], but the known increase in δ with [SDS] [42] implies a constant coupling strength β.

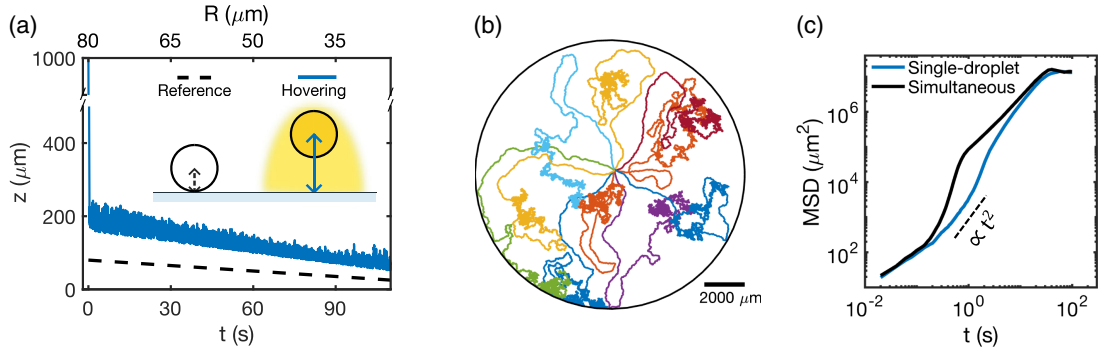

FIG. 5. Extensions to the model using parameters from the MSD fit in Fig. 2(b). (a) A simulated active droplet rapidly falls to its equilibrium hovering height around $z = 200$ μm. The dashed line shows the shrinking radius on the surface for reference. (b) Multiple droplets are injected simultaneously in the center of the sample cell. (c) Their $\mathrm{MSD}^{\mathrm{ens}}$ is enhanced compared to that of single droplets due to their repulsive interactions at the center.

Acknowledgments—The authors thank Sébastien Michelin, Sascha Hilgenfeldt, Katherine A. Newhall, and John Brady for their enlightening discussions. E. V.-E. is supported by the National Science Foundation (NSF) DMR-1420073, DMS-2012510, and DMS-2134216, by the Simons Collaboration on Wave Turbulence, Grant No. 617006, and by a Vannevar Bush Faculty Fellowship. J. B. is supported by the NSF DMR Grant No. 2105255 and the Swiss National Science Foundation through Grant No. 10000141.

[1] J. Adler, Science **153**, 708 (1966).
[2] G. L. Hazelbauer, Annu. Rev. Microbiol. **66**, 285 (2012).
[3] N. Mittal, E. O. Budrene, M. P. Brenner, and A. Van Oudenaarden, Proc. Natl. Acad. Sci. U.S.A. **100**, 13259 (2003).
[4] C. C. Maass, C. Krüger, S. Herminghaus, and C. Bahr, Annu. Rev. Condens. Matter Phys. **7**, 171 (2016).
[5] J. L. Moran and J. D. Posner, Annu. Rev. Fluid Mech. **49**, 511 (2017).
[6] D. Lohse and X. Zhang, Nat. Rev. Phys. **2**, 426 (2020).
[7] S. Michelin, Annu. Rev. Fluid Mech. **55**, 77 (2023).
[8] C. Krüger, G. Klös, C. Bahr, and C. C. Maass, Phys. Rev. Lett. **117**, 048003 (2016).
[9] P. Ramesh, Y. Chen, P. Räder, S. Morsbach, M. Jalaal, and C. C. Maass, arXiv:2303.13442.
[10] B. V. Hokmabad, R. Dey, M. Jalaal, D. Mohanty, M. Almukambetova, K. A. Baldwin, D. Lohse, and C. C. Maass, Phys. Rev. X **11**, 011043 (2021).
[11] P. Dwivedi, A. Shrivastava, D. Pillai, and R. Mangal, Soft Matter **19**, 4099 (2023).
[12] M. Suga, S. Suda, M. Ichikawa, and Y. Kimura, Phys. Rev. E **97**, 062703 (2018).
[13] S. Suda, T. Suda, T. Ohmura, and M. Ichikawa, Phys. Rev. Lett. **127**, 088005 (2021).
[14] S. Ray and A. Roy, Liq. Cryst. 1 (2024); arXiv:2410.14438.
[15] A. Izzet, P. G. Moerman, P. Gross, J. Groenewold, A. D. Hollingsworth, J. Bibette, and J. Brujic, Phys. Rev. X **10**, 021035 (2020).
[16] R. Dey, C. M. Buness, B. V. Hokmabad, C. Jin, and C. C. Maass, Nat. Commun. **13**, 2952 (2022).
[17] B. Schulz, S. Trimper, and M. Schulz, Phys. Lett. A **339**, 224 (2005).
[18] B. V. Hokmabad, J. Agudo-Canalejo, S. Saha, R. Golestanian, and C. C. Maass, Proc. Natl. Acad. Sci. U.S.A. **119**, e2122269119 (2022).
[19] C. Jin, C. Krüger, and C. C. Maass, Proc. Natl. Acad. Sci. U.S.A. **114**, 5089 (2017).
[20] P. G. Moerman, H. W. Moyses, E. B. Van Der Wee, D. G. Grier, A. Van Blaaderen, W. K. Kegel, J. Groenewold, and J. Brujic, Phys. Rev. E **96**, 032607 (2017).
[21] P. J. Flory, *Principles of Polymer Chemistry* (Cornell University Press, Ithaca, 1953).
[22] S. E. Derkachov, J. Honkonen, E. Karjalainen, and A. N. Vasil'ev, J. Phys. A **22**, L385 (1989).
[23] P. Grassberger, Phys. Rev. Lett. **119**, 140601 (2017).
[24] A. Barbier-Chebbah, O. Bénichou, and R. Voituriez, Phys. Rev. X **12**, 011052 (2022).
[25] Y. Tsori and P.-G. De Gennes, Europhys. Lett. **66**, 599 (2004).
[26] R. Grima, Phys. Rev. Lett. **95**, 128103 (2005).
[27] R. Grima, Phys. Rev. E **74**, 011125 (2006).
[28] A. Sengupta, S. van Teeffelen, and H. Löwen, Phys. Rev. E **80**, 031122 (2009).
[29] J. Taktikos, V. Zaburdaev, and H. Stark, Phys. Rev. E **84**, 041924 (2011).
[30] W. T. Kranz, A. Gelimson, K. Zhao, G. C. Wong, and R. Golestanian, Phys. Rev. Lett. **117**, 038101 (2016).
[31] K. Daftari and K. A. Newhall, Phys. Rev. E **105**, 024609 (2022).
[32] K. Daftari and K. Newhall, arXiv:2403.19393.
[33] C. Jin, J. Vachier, S. Bandyopadhyay, T. Macharashvili, and C. C. Maass, Phys. Rev. E **100**, 040601(R) (2019).
[34] C. de Blois, M. Reyssat, S. Michelin, and O. Dauchot, Phys. Rev. Fluids **4**, 054001 (2019).
[35] P. J. Missel, N. Mazer, G. Benedek, C. Young, and M. C. Carey, J. Phys. Chem. **84**, 1044 (1980).
[36] P. C. Hiemenz and R. Rajagopalan, *Principles of Colloid and Surface Chemistry, Revised and Expanded* (CRC Press, Boca Raton, 2016).
[37] See Supplemental Material at http://link.aps.org/supplemental/10.1103/PhysRevLett.134.018301 for additional information.
[38] M. Morozov and S. Michelin, J. Chem. Phys. **150** (2019).

[39] M. Schmitt and H. Stark, Europhys. Lett. **101**, 44008 (2013).
[40] M. Schmitt and H. Stark, Phys. Fluids **28** (2016).
[41] D. J. Amit, G. Parisi, and L. Peliti, Phys. Rev. B **27**, 1635 (1983).
[42] M. Pisárčik, F. Devínsky, and M. Pupák, Open Chem. **13**, 922 (2015).
[43] W.-F. Hu, T.-S. Lin, S. Rafai, and C. Misbah, Phys. Rev. Lett. **123**, 238004 (2019).
[44] W.-F. Hu, T.-S. Lin, S. Rafai, and C. Misbah, Phys. Rev. Fluids **7**, 034003 (2022).
[45] V. Y. Bezzobotnov, S. Borbely, L. Cser, B. Farago, I. Gladkih, Y. M. Ostanevich, and S. Vass, J. Phys. Chem. **92**, 5738 (1988).
[46] N. Christov, N. Denkov, P. Kralchevsky, K. Ananthapadmanabhan, and A. Lips, Langmuir **20**, 565 (2004).
[47] A. C. Castonguay, R. Kailasham, C. M. Wentworth, C. H. Meredith, A. S. Khair, and L. D. Zarzar, Phys. Rev. E **107**, 024608 (2023).
[48] N. Desai and S. Michelin, Phys. Rev. Fluids **6**, 114103 (2021).